Published in final edited form as:
Nano Lett. 2011 June 8; 11(6): 2560–2566. doi:10.1021/nl201400z.

Copper Selenide Nanocrystals for Photothermal Therapy

Colin M. Hessel[†], **Varun Pattani**[‡], **Michael Rasch**[†], **Matthew G. Panthani**[†], **Bonil Koo**[§], **James W. Tunnell**[‡], and **Brian A. Korgel**[†,*]

[†]Department of Chemical Engineering, Texas Materials Institute, and Center for Nano- and Molecular Science and Technology, Austin, Texas 78712

[‡]Department of Biomedical Engineering, The University of Texas at Austin; Austin, Texas 78712

[§]Argonne National Laboratory Center for Nanoscale Materials 9700 S. Cass Ave, Building 440 Argonne, IL 60439

Abstract

Ligand-stabilized copper selenide ($Cu_{2-x}Se$) nanocrystals, approximately 16 nm in diameter, were synthesized by a colloidal hot injection method and coated with amphiphilic polymer. The nanocrystals readily disperse in water and exhibit strong near infrared (NIR) optical absorption with a high molar extinction coefficient of 7.7×10^7 cm^{-1} M^{-1} at 980 nm. When excited with 800 nm light, the $Cu_{2-x}Se$ nanocrystals produce significant photothermal heating with a photothermal transduction efficiency of 22%, comparable to nanorods and nanoshells of gold (Au). *In vitro* photothermal heating of $Cu_{2-x}Se$ nanocrystals in the presence of human colorectal cancer cell (HCT-116) led to cell destruction after 5 minutes of laser irradiation at 33 W/cm^2, demonstrating the viabilitiy of $Cu_{2-x}Se$ nanocrystals for photothermal therapy applications.

Keywords

copper selenide; photothermal therapy (PPT); plasmon resonance; colloidal nanocrystals; amphiphilic polymer; cancer therapy; hyperthermia; gold nanoshells; gold nanorods; photothermal transduction efficiency

There is growing interest in combating cancer with nanoparticle-based therapeutics.[1] Photoinduced heating of nanoparticles using near infrared (NIR) light to destroy cancer cells has been shown to be a potentially effective way to target cell death without damaging surrounding healthy tissue.[2–4] The nanoparticles should be smaller than about 50 nm or so, non-toxic, and have surfaces that can be functionalized with cell recognition moieties. Furthermore, the nanoparticles should respond strongly to light excitation with wavelengths in the range of 650 to 950 nm, due to the high transparency of tissue, blood, and water in this range of wavelengths.[5]

Gold (Au) nanoshells,[6] nanorods,[7] and nanocages,[8, 9] have high optical extinction coefficients in the NIR wavelength range with size- and shape-tunable surface plasmon resonance (SPR) bands that can be photoexcited to generate considerable heat. Therefore, they have been widely studied for optical diagnostic imaging and photothermal therapy. Au nanorods and nanoshells, however, can be considerably large—Au nanorods are typically on

*Corresponding author: (T) +1-512-471-5633; (F) +1-512-471-7060; korgel@che.utexas.edu.

SUPPORTING INFORMATION Detailed methods and descriptions of the experiments associated with the synthesis and characterization of $Cu_{2-x}Se$, Au nanoshells and Au nanorods, in addition to cytotoxicity and cell death studies. This material is available free of charge via the Internet at http://pubs.acs.org.

the order of ~10 nm in diameter and ~ 50 nm in length,[10] and Au nanoshells are more than 100 nm in diameter.[11–13] The optimum intravenously administered nanoparticles should be between 10 and 50 nm in diameter to increase blood stream circulation time,[14–16] as larger nanoparticles are removed by the reticuloendothelial system, primarily by the liver and spleen, and smaller particles by the renal system.[17–19] Furthermore, the cetyltrimethylammonium bromide (CTAB) coating on Au nanorods is cytotoxic and not easily removed without losing the integrity of the material.[12]

Other nanomaterials including germanium nanocrystals,[20] porous silicon,[21] graphene flakes,[22] carbon nanotubes,[4, 23] copper(II) sulfide nanocrystals,[24] and graphitic carbon coated iron cobalt nanocrystals[25] have also been shown to generate sufficient photothermal heating by NIR optical illumination to destroy cancer cells. Nonetheless, there is still a need for photothermal nanoparticles in the right size range and adequate cell biocompatibility. Copper-based semiconductors have recently gained recognition as biocompatible alternatives to Cd-containing contrast agents (e.g. CdS, CdSe, CdTe) for *in vivo* cancer imaging applications.[24,26] $CuInS_2$@ZnS and $CuInSe_2$@ZnS core-shell nanocrystals have shown bioimaging efficacy comparable to the Cd-based materials, without the toxicity associated with Cd,[27–29] and recently copper (II) sulfide nanocrystals were explored for photothermal therapy, although with reportedly limited photothermal transduction efficiency.[24] In this *Letter*, we show that $Cu_{2-x}Se$ nanocrystals are an effective photothermal material, exhibiting marked photo-induced heating when excited by NIR light at 800 nm and similar photothermal transduction efficiency as Au nanorods and Au nanoshells. Human colorectal cancer cell death is also observed by *in situ* laser-induced photothermal heating of $Cu_{2-x}Se$ nanocrystals.

$Cu_{2-x}Se$ nanocrystals were synthesized by arrested precipitation in a hot organic solvent and coated with amphiphilic polymer to be rendered hydrophilic and compatible with biological systems. Based on a modification of methods developed for $CuInS_2$ and $Cu(InxGa_{1-x})Se_2$ nanocrystals,[30, 31] two hot reactant solutions of copper chloride and selenourea in oleylamine are combined to form a dark green colloidal dispersion of oleylamine-capped $Cu_{2-x}Se$ nanocrystals, as in Figure 1 (see Supporting Information for experimental details). Transmission electron microscopy (TEM) images show that the nanocrystals are predominantly spherical in shape with crystalline cores of an average diameter of 16±1 nm. The $Cu_{2-x}Se$ nanocrystals typically had copper selenide, photothermal therapy (PPT), plasmon resonance, colloidal nanocrystals, amphiphilic polymer, cancer therapy, hyperthermia, gold nanoshells, gold nanorods, photothermal transduction efficiency

There is growing interest in combating cancer with nanoparticle-based therapeutics.[1] Photoinduced heating of nanoparticles using near infrared (NIR) light to destroy cancer cells has been shown to be a potentially effective way to target cell death without damaging surrounding healthy tissue.[2–4] The nanoparticles should be smaller than about 50 nm or so, non-toxic, and have surfaces that can be functionalized with cell recognition moieties. Furthermore, the nanoparticles should respond strongly to light excitation with wavelengths in the range of 650 to 950 nm, due to the high transparency of tissue, blood, and water in this range of wavelengths.[5]

Gold (Au) nanoshells,[6] nanorods,[7] and nanocages,[8, 9] have high optical extinction coefficients in the NIR wavelength range with size- and shape-tunable surface plasmon resonance (SPR) bands that can be photoexcited to generate considerable heat. Therefore, they have been widely studied for optical diagnostic imaging and photothermal therapy. Au nanorods and nanoshells, however, can be considerably large—Au nanorods are typically on the order of ~10 nm in diameter and ~ 50 nm in length,[10] and Au nanoshells are more than 100 nm in diameter.[11–13] The optimum intravenously administered nanoparticles should be

between 10 and 50 nm in diameter to increase blood stream circulation time,[14–16] as larger nanoparticles are removed by the reticuloendothelial system, primarily by the liver and spleen, and smaller particles by the renal system.[17–19] Furthermore, the cetyltrimethylammonium bromide (CTAB) coating on Au nanorods is cytotoxic and not easily removed without losing the integrity of the material.[12]

The hydrophobic oleylamine-capped nanocrystals were coated with amphiphilic polymer composed of a poly(maleic anhydride) backbone with hydrophilic carboxylic acid groups and hydrophobic oleylamine side chains (Figure 2) using techniques described previously.[33] The polymer forms micelles in water, which encapsulate the nanocrystals. The amphiphilic polymer coating enables dispersion of the nanocrystals in aqueous media under physiological conditions i.e., phosphate buffered saline (PBS) at pH 7.4 and 150 mM,[33] and the distal carboxyl groups can be further functionalized with cellular targeting biomolecules such as proteins or antibodies.[34, 35] With the polymer coating, the $Cu_{2-x}Se$ nanocrystals have an average hydrodynamic diameter and zeta potential of 39 nm and −40 mV, respectively, which makes them well-suited for in vivo medical applications.

Figure 3 shows room temperature UV-vis-NIR absorbance spectra of $Cu_{2-x}Se$ nanocrystals dispersed in water. There is a broad absorbance peak centered at 970 nm with monotonically rising absorbance at wavelengths below 500 nm. Similar absorbance features were observed by Manna and coworkers[32] and Garcia and coworkers[36] and were assigned to direct and indirect interband transitions for $Cu_{2-x}Se$. Bulk $Cu_{2-x}Se$ has direct and indirect band gap energies of 2.1 to 2.3 eV (540 to 590 nm) and 1.2 to 1.4 eV (1030 to 880 nm), respectively. We also assign the low wavelength (less than approximately 600 nm) absorbance to interband optical transitions; however, we assign the NIR absorbance peak to a surface plasmon resonance. $Cu_{2-x}Se$ is a p-type semiconductor with a relatively high carrier (holes) concentration and exhibits strong free carrier absorption,[37] which in the case of the $Cu_{2-x}Se$ nanocrystals results in a surface plasmon resonance. Nanocrystals of analogous non-stoichiometric copper sulfides ($Cu_{2-x}S$)—in which Cu deficiencies also lead to high densities of holes—have also exhibited NIR absorbance peaks.[38–40] The NIR absorption band from $Cu_{2-x}S$ was also originally assigned to an indirect interband transition;[38, 39] however, Burda and coworkers have clarified using Drude theory that the NIR absorption is actually a surface plasmon resonance.[40] Very recently, Luther and coworkers revealed that $Cu_{2-x}S$ nanocrystals with vacancy concentrations of ~10^{21} cm^{-3} exhibit surface plasmon resonance bands, thus confiming that substoichiometric copper (I) chalcogenides have absorption characteristics similar to those of metals.[41] The high molar extinction coefficients measured for the $Cu_{2-x}Se$ nanocrystals (with a value of 7.7×10^7 $M^{-1}cm^{-1}$ (at 970 nm)) are also consistent with plasmon absorption,[41] and are orders of magnitude higher than expected for an indirect optical transition and considerably higher than strongly absorbing organic dyes, direct bandgap semiconductor quantum dots (See Table 1).

A significant amount of heat was observed to evolve when the NIR plasmon resonance was optically excited. Photothermal heating of $Cu_{2-x}Se$ nanocrystals was measured by irradiating an aqueous dispersion with 800 nm light near the plasmon band at low fluence (2 W/cm^2) for 5 min. The optical density of the nanocrystal dispersion was adjusted to 1.0 at the excitation wavelength. Figure 5B shows the temperature of the dispersion as a function of irradiation time. Five minutes of light exposure raised the temperature by 22°C, which compares quite favorably with the photothermal heating of Au nanoshells and Au nanorods synthesized in-house (see Supporting Information for experimental details and Figure 5 for TEM characterization)[13, 47] and obtained commercially. As shown in Figure 4, under similar illumination conditions, with the optical densities of the Au nanorods and nanoshells also adjusted to 1.0 at the excitation wavelength of 800 nm to normalize the photothermal responses of all of the materials, the Au nanoshells increased the temperature by 13°C

(synthesized) and 15°C (commercial), and Au nanorods by 20°C (synthesized) and 22°C (commercial) after 5 minutes.

The photothermal transduction efficiencies of the $Cu_{2-x}Se$ nanocrystals and the commercial gold-based nanoparticles were also measured and found to be quite similar. Similar to Roper and coworkers,[48] nanoparticle dispersions were illuminated until reaching a steady-state temperature increase. The light source was then removed and the temperature decrease was monitored to determine the rate of heat transfer from the system. Figure 6 shows the typical thermal profiles of the different nanoparticles. From an energy balance on the system, the photothermal transduction efficiency could be calculated. The total energy balance for the system is

$$\Sigma_i m_i C_{p,i} \frac{dT}{dt} = Q_{in,np} + Q_{in,surr} - Q_{out} \quad (1)$$

where m and C_p are the mass and heat capacity of the solvent (water) and T is the solution temperature. $Q_{in,np}$ is the photothermal energy input from the nanocrystals:

$$Q_{in,np} = I\left(1 - 10^{(-A_\lambda)}\right)\eta \quad (2)$$

where I is the laser power (in units of mW), A_λ is the absorbance at the excitation wavelength of 800 nm, and η is the photothermal transduction efficiency, or the fraction of absorbed light energy that is converted to heat. $Q_{in,surr}$ is the heat input (in units of mW) due to light absorption by the solvent, which was measured independently and found to be 25.1 mW. Q_{out} is the heat lost to the surroundings:

$$Q_{out} = hA\,(T - T_{surr}) \quad (3)$$

where h is the heat transfer coefficient, A is the surface area of the container, and T_{surr} is the ambient surrounding temperature. The lumped quantity hA, was determined by measuring the rate of temperature drop after removing the light source. In the absence of any laser excitation, Eqn (1) becomes

$$\Sigma_i m_i C_{p,i} \frac{dT}{dt} = -Q_{out} = -hA\,(T - T_{surr}) \quad (4)$$

Rearranging Eqn (4),

$$dt = -\frac{m_{H_2O} C_{p,H_2O}}{hA} \frac{dT}{(T - T_{surr})} \quad (5)$$

and integrating, gives the expression

$$t = -\left(\frac{m_{H_2O} C_{p,H_2O}}{hA}\right) \ln\,(T - T_{surr}) \quad (6)$$

A characteristic rate constant can then be defined, $\tau_{out} = m_{H2O}C_{p,H2O}/hA$, such that

$$T - T_{surr} = \exp\left(-\frac{hA}{m_{H_2O} C_{p,H_2O}} t\right) = \exp\left(-\frac{t}{\tau_{out}}\right) \quad (7)$$

From the data in Figure 6, τ_{out} and heat transfer coefficients (hA) were found for each solution during solution heating and cooling, and are tabulated in Table SI 2. At the maximum steady-state temperature, the rate of photothermal heating is then equal to the rate of heat transfer out of the system:

$$Q_{in,np} + Q_{in,surr} = I\left(1 - 10^{(-A_\lambda)}\right)\eta + Q_{in,surr} = hA\,(T_{\max} - T_{surr}) \quad (8)$$

where T_{max} is the maximum steady-state temperature. Therefore, the photothermal transduction efficiency can be calculated directly from the steady-state temperature increase, since

$$\eta = \frac{hA\,(T_{\max} - T_{surr}) - Q_{in,surr}}{I\left(1 - 10^{(-A_\lambda)}\right)} \quad (9)$$

Figure 6B shows the photothermal transduction efficiencies measured for the $Cu_{2-x}Se$ nanocrystals (22%), and commercial Au nanoshells (13%) and nanorods (21%).

The photothermal transduction efficiency of the $Cu_{2-x}Se$ nanocrystals of 22% is nearly equivalent to Au nanorods (21%) and noticeably higher than Au nanoshells (13%). Halas and coworkers have reported similar differences in the photothermal transduction efficiencies between Au nanoshells and nanorods, and have shown the amount of heat generated experimentally is almost three fold less than what is theoretically predicted.[49] The lower η for Au nanoshells compared to the nanorods and $Cu_{2-x}Se$ nanocrystals is due to the larger contribution of light scattering to the optical cross-section that does not contribute to heating. Since the nanoparticle dispersions had the same optical density at the excitation wavelength, the same amount of light was attenuated in each measurement (Figure 5B). However, the Au nanoshells are significantly larger ($r_{nanoshell}$ = 72.5 nm) than the Au nanorods ($r_{eff,nanorod}$ = 8.7 nm) and $Cu_{2-x}Se$ nanocrystals (r = 8 nm). The size-dependence of the extinction coefficient and the relative amounts of light scattering and absorption have been extensively studied for Au nanostructures and is well understood.[50–52] El-Sayed and coworkers for example have illustrated how particle size affects the plasmonic properties of gold nanoparticles by normalizing the extinction coefficient to the particle volume (in units of μm^3) and considering the relative contributions from light absorption and scattering.[44] They have observed that Au nanorods have a normalized extinction coefficient (μ_{ext}) of 1021.05 μm^{-1}, which is the sum of normalized absorption (μ_{abs} = 986.56 μm^{-1}) and scattering (μ_{sca} = 34.49 μm^{-1}) coefficients, and that Au nanoshells have a normalized extinction coefficient of 58.39 μm^{-1}, which is the sum of normalized absorption and scattering coefficients of 35.66 μm^{-1} and 22.73 μm^{-1}, respectively. Therefore, the higher photothermal efficiency of nanorods compared to nanoshells is consistent with their higher absorption compared to scattering (96% vs. 60%, respectively).[44] Like the Au nanorods, the $Cu_{2-x}Se$ nanocrystals are small enough that the majority of optical extinction is due to light absorption related to the plasmon resonance.

The biocompatibility of the polymer-coated $Cu_{2-x}Se$ nanocrystals was tested by conducting a cell viability assay of human colorectal carcinoma HCT-116 cells in the presence of the

nanocrystals. Cells were cultured until a confluency of 80% was reached and charged with a combination of new media and $Cu_{2-x}Se$ dispersed in PBS to give a solution concentration of 39 mg/L (2.8×10^{15} NCs/L, equivalent concentration to 0.25 OD by absorbance spectroscopy). Cells were incubated for 0.5 hr, 1 hr, 3 hr, and 6 hr at 37°C. Control cells received fresh nanoparticle-free media and were incubated as well for 6 hr. The media was replaced after incubation to remove all unbound nanoparticles and Trypan blue, a membrane permeability stain, was added to assess cell death. Dead cells absorb dye and appear blue, whereas viable cells are clear under a brightfield microscope. Figure 7 shows bright field images of HCT-116 cells after incubation with polymer-coated $Cu_{2-x}Se$ nanocrystals. The cell viability assay indicates that incubation of HCT-116 cells with the nanocrystals show no signs of cytotoxicity up to 6 hr, and only a slight increase in cell death at 6 hr compared to the control. Additional long-term cytoxoticity studies are underway.

$Cu_{2-x}Se$ nanocrystals were added to HCT-116 cells and illuminated with 800 nm light to determine if they would promote photothermal cell death. In photothermal therapy, NIR light is used to excite the nanocrystals and create local temperature increases to destroy diseased cells. Heat-induced protein denaturation occurs above 40°C, which leads to cell death/injury,[53, 54] and RNA and DNA unfold at temperatures above 85–90°C.[55] Cells grown in a 12-well plate were combined with media (0.375 mL) and $Cu_{2-x}Se$ nanocrystals in PBS (0.125 mL) at a solution concentration of 39 mg/L (2.8×10^{15} NCs/L) and were incubated for 0.5 hr at 37°C. Cells were irradiated for five minutes with and without $Cu_{2-x}Se$ nanocrystals at 30 W/cm^2. Bright field imaging of cells stained with Trypan Blue after irradiation (Figure 8 – bottom row) show that all of the cells exposed to nanocrystals exhibited photothermal cell destruction. Exposure of the cells to the NIR laser in the absence of nanocrystals did not compromise cell viability (Figure 8). The power threshold for non-targeted photothermal cell destruction using an 800 nm laser was 30 W/cm^2 for 5 min. These conditions are slightly more moderate than what is reported for non-targeted *in vitro* photothermal cell destruction with Au nanoshells (35 W/cm^2, 7 min) or targeted *in vitro* photothermal therapy with hollow Au nanoshells (40 W/cm^2, 5 min).[56]

Conclusions

Amphiphilic polymer-coated $Cu_{2-x}Se$ nanocrystals exhibit an intense NIR absorbance peak and significant photothermal heating, comparable to Au nanorods and nanoshells. NIR photoexcitation of the $Cu_{2-x}Se$ nanocrystals in the presence of human colorectal cancer cells led to significant cell death, verifying that the nanocrystals have the potential for photothermal therapy. The potential for $Cu_{2-x}Se$ as an *in vivo* therapeutic is highlighted by its small hydrodynamic diameter that will lead to prolonged blood circulation times when additional non-immunogenic or cellular targeting molecules are attached for targeted photothermal therapy.

Supplementary Material

Refer to Web version on PubMed Central for supplementary material.

Acknowledgments

We acknowledge the National Science Foundation (Grant No. 0618242), The Robert A. Welch Foundation (Grant No.F-1464), the National Institutes of Health (Grant No. R01 CA132032), and the Natural Science and Engineering Research Council of Canada for financial support of this work. We also thank José L.Hueso for synthesizing gold nanorods and Nanospectra Biosciences for providing the commercial Au nanoshells and Au nanorods.

References

1. Jain PK, El-Sayed IH, El-Sayed MA. Nano Today. 2007; 2:18–29.
2. Huang XH, El-Sayed IH, Qian W, El-Sayed MA. J. Am. Chem. Soc. 2006; 128:2115–2120. [PubMed: 16464114]
3. Gobin AM, Lee MH, Halas NJ, James WD, Drezek RA, West JL. Nano Lett. 2007; 7:1929–1934. [PubMed: 17550297]
4. Kam NWS, O'Connell M, Wisdom JA, Dai HJ. Proc. Natl. Acad. Sci. U. S. A. 2005; 102:11600–11605. [PubMed: 16087878]
5. Weissleder R. Nat. Biotechnol. 2001; 19:316–317. [PubMed: 11283581]
6. Oldenburg SJ, Averitt RD, Westcott SL, Halas NJ. Chem. Phys. Lett. 1998; 288:243–247.
7. Huang XH, Neretina S, El-Sayed MA. Adv. Mater. 2009; 21:4880–4910.
8. Chen JY, Wang DL, Xi JF, Au L, Siekkinen A, Warsen A, Li ZY, Zhang H, Xia YN, Li XD. Nano Lett. 2007; 7:1318–1322. [PubMed: 17430005]
9. Chen JY, Glaus C, Laforest R, Zhang Q, Yang MX, Gidding M, Welch MJ, Xia YN. Small. 2010; 6:811–817. [PubMed: 20225187]
10. Nikoobakht B, El-Sayed MA. Chem. Mater. 2003; 15:1957–1962.
11. Loo C, Lin A, Hirsch L, Lee MH, Barton J, Halas NJ, West J, Drezek R. Technol. Cancer Res. Treat. 2004; 3:33–40. [PubMed: 14750891]
12. Alkilany AM, Nagaria PK, Hexel CR, Shaw TJ, Murphy CJ, Wyatt MD. Small. 2009; 5:701–708. [PubMed: 19226599]
13. Rasch MR, Sokolov KV, Korgel BA. Langmuir. 2009; 25:11777–11785. [PubMed: 19711913]
14. Soo, Choi, H.; Liu, W.; Misra, P.; Tanaka, E.; Zimmer, JP.; Itty, Ipe, B.; Bawendi, MG.; Frangioni, JV. Nat. Biotechnol. 2007; 25:1165–1170. [PubMed: 17891134]
15. Jiang W, Kim BYS, Rutka JT, Chan WCW. Nat. Nanotechnol. 2008; 3:145–150. [PubMed: 18654486]
16. Gao H, Shi W, Freund LB. Proc. Natl. Acad. Sci. USA. 2005; 102:9469–9474. [PubMed: 15972807]
17. Osaki F, Kanamori T, Sando S, Sera T, Aoyama Y. J. Am. Chem. Soc. 2004; 126:6520–6521. [PubMed: 15161257]
18. Sadauskas E, Wallin H, Stoltenberg M, Vogel U, Doering P, Larsen A, Danscher G. Part. Fibre Toxicol. 2007; 4:10–17. [PubMed: 17949501]
19. De Jong WH, Hagens WI, Krystek P, Burger MC, Sips A, Geertsma RE. Biomaterials. 2008; 29:1912–1919. [PubMed: 18242692]
20. Lambert TN, Andrews NL, Gerung H, Boyle TJ, Oliver JM, Wilson BS, Han SM. Small. 2007; 3:691–699. [PubMed: 17299826]
21. Lee C, Kim H, Hong C, Kim M, Hong SS, Lee DH, Lee WI. J. Mater. Chem. 2008; 18:4790–4795.
22. Yang K, Zhang SA, Zhang GX, Sun XM, Lee ST, Liu ZA. Nano Lett. 2010; 10:3318–3323. [PubMed: 20684528]
23. Moon HK, Lee SH, Choi HC. ACS Nano. 2009; 3:3707–3713. [PubMed: 19877694]
24. Li YB, Lu W, Huang QA, Huang MA, Li C, Chen W. Nanomedicine. 2010; 5:1161–1171. [PubMed: 21039194]
25. Sherlock SP, Tabakman SM, Xie L, Dai H. ACS Nano. 2011; 5:1505–1512. [PubMed: 21284398]
26. Derfus AM, Chan WCW, Bhatia SN. Nano Lett. 2004; 4:11–18.
27. Li L, Daou TJ, Texier I, Tran TKC, Nguyen QL, Reiss P. Chem. Mater. 2009; 21:2422–2429.
28. Pons T, Pic E, Lequeux N, Cassette E, Bezdetnaya L, Guillemin F, Marchal F, Dubertret B. ACS Nano. 2010; 4:2531–2538. [PubMed: 20387796]
29. Cassette E, Pons T, Bouet C, Helle M, Bezdetnaya L, Marchal F, Dubertret B. Chem. Mater. 2010; 22:6117–6124.
30. Panthani MG, Akhavan V, Goodfellow B, Schmidtke JP, Dunn L, Dodabalapur A, Barbara PF, Korgel BA. J. Am. Chem. Soc. 2008; 130:16770–16777. [PubMed: 19049468]
31. Koo B, Patel RN, Korgel BA. J. Am. Chem. Soc. 2009; 131:3134–3135. [PubMed: 19216573]

32. Deka S, Genovese A, Zhang Y, Miszta K, Bertoni G, Krahne R, Giannini C, Manna L. J. Am. Chem. Soc. 2010; 132:8912–8914. [PubMed: 20540521]
33. Hessel CM, Rasch MR, Hueso JL, Goodfellow BW, Akhavan VA, Puvanakrishnan P, Tunnel JW, Korgel BA. Small. 2010; 6:2026–2034. [PubMed: 20818646]
34. Franchina JG, Lackowski WM, Dermody DL, Crooks RM, Bergbreiter DE, Sirkar K, Russell RJ, Pishko MV. Anal. Chem. 1999; 71:3133–3139. [PubMed: 10450159]
35. Li ZF, Kang ET, Neoh KG, Tan KL. Biomaterials. 1998; 19:45–53. [PubMed: 9678849]
36. Garcia VM, Nair PK, Nair MTS. J. Cryst. Growth. 1999; 203:113–124.
37. Jagminas A, Juskenas R, Gailiute I, Statkute G, Tomasiunas R. J. Cryst. Growth. 2006; 294:343–348.
38. Kuzuya T, Itoh K, Sumiyama K. J. Colloid Interface Sci. 2008; 319:565–571. [PubMed: 18155227]
39. Klimov V, Bolivar PH, Kurz H, Karavanskii V, Krasovskii V, Korkishko Y. Appl. Phys. Lett. 1995; 67:653–655.
40. Zhao Y, Pan H, Lou Y, Qiu X, Zhu J, Burda C. J. Am. Chem. Soc. 2009; 131:4253–4261. [PubMed: 19267472]
41. Luther JM, Jain PK, Ewers T, Alivisatos AP. Nat. Mater. 2011; 10:361–366. [PubMed: 21478881]
42. Du H, Fuh RCA, Li JZ, Corkan LA, Lindsey JS. Photochem. Photobiol. 1998; 68:141–142.
43. Yu WW, Qu LH, Guo WZ, Peng XG. Chem. Mater. 2003; 15:2854–2860.
44. Jain PK, Lee KS, El-Sayed IH, El-Sayed MA. J. Phys. Chem. B. 2006; 110:7238–7248. [PubMed: 16599493]
45. Nikoobakht B, Wang JP, El-Sayed MA. Chem. Phys. Lett. 2002; 366:17–23.
46. Hirsch LR, Stafford RJ, Bankson JA, Sershen SR, Rivera B, Price RE, Hazle JD, Halas NJ, West JL. Proc. Natl. Acad. Sci. U. S. A. 2003; 100:13549–13554. [PubMed: 14597719]
47. Smith DK, Miller NR, Korgel BA. Langmuir. 2009; 25:9518–9524. [PubMed: 19413325]
48. Roper DK, Ahn W, Hoepfner M. J. Phys. Chem. C. 2007; 111:3636–3641.
49. Cole JR, Mirin NA, Knight MW, Goodrich GP, Halas NJ. J. Phys. Chem. C. 2009; 113:12090–12094.
50. Link S, El-Sayed MA. J. Phys. Chem. B. 1999; 103:8410–8426.
51. Link S, El-Sayed MA. Int. Rev. Phys. Chem. 2000; 19:409–453.
52. Bohren, CF.; Huffman, DR. Absorption and Scattering of Light by Small Particles. John Wiley; New York: 1983.
53. He XM, Wolkers WF, Crowe JH, Swanlund DJ, Bischof JC. Ann. Biomed. Eng. 2004; 32:1384–1398. [PubMed: 15535056]
54. Lepock JR. Int. J. Hyperthermia. 2003; 19:252–266. [PubMed: 12745971]
55. Lepock JR. Radiat. Res. 1982; 92:433–438. [PubMed: 7178412]
56. Melancon MP, Lu W, Yang Z, Zhang R, Cheng Z, Elliot AM, Stafford J, Olson T, Zhang JZ, Li C. Mol. Cancer Ther. 2008; 7:1730–1739. [PubMed: 18566244]

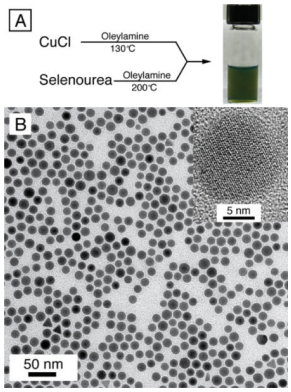

Figure 1.

(A) Reaction scheme and a photograph of oleylamine-capped $Cu_{2-x}Se$ nanocrystals dispersed in chloroform; (B) TEM images of copper selenide nanocrystals. The high resolution TEM image in the inset of (B) shows the crystalline $Cu_{2-x}Se$ core of the nanocrystals. The average diameter of the nanocrystals is 16±1 nm.

NIH-PA Author Manuscript

NIH-PA Author Manuscript

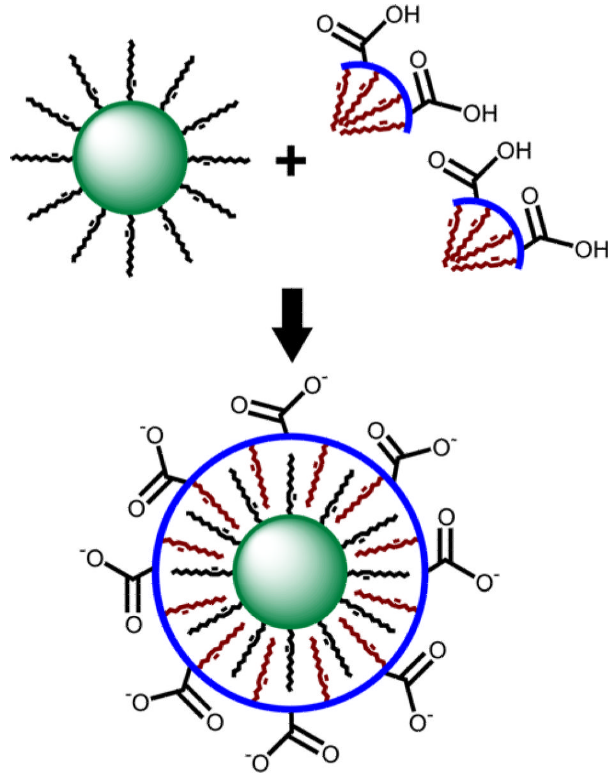

Figure 2.

Amphiphilic polymer encapsulation of $Cu_{2-x}Se$ nanocrystals. Combining oleylamine passivated $Cu_{2-x}Se$ nanocrystals and the amphiphilic poly(maleic anhydride)-based polymer leads to encapsulation of the $Cu_{2-x}Se$ nanocrystals with a hydrophilic exterior. The distal carboxyl groups on the surface facilitate dispersibility in aqueous media.

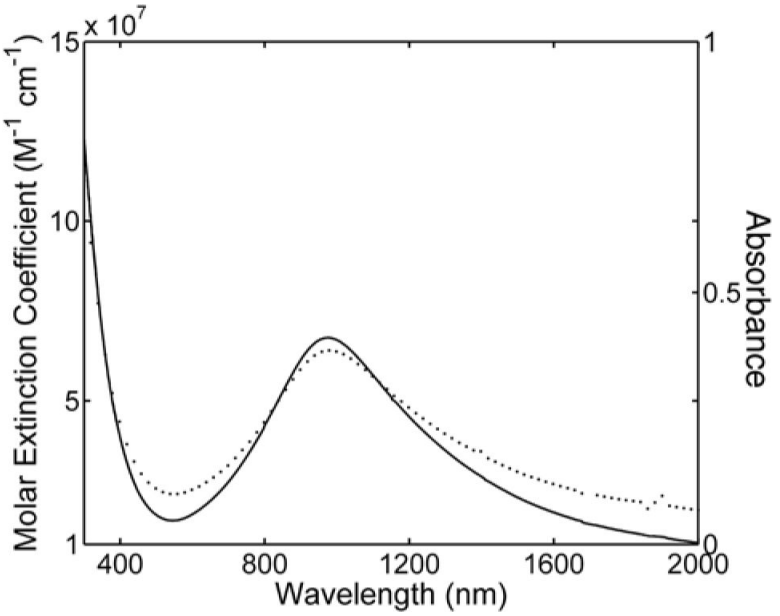

Figure 3.

Absorbance (dotted line) and molar extinction coefficient (solid line) for $Cu_{2-x}Se$ nanocrystals plotted against wavelength. The absorbance spectrum of polymer coated $Cu_{2-x}Se$ nanocrystals in water (37 mg/L) reaches a maximum at 970 nm. The molar extinction coefficient was calculated experimentally using $Cu_{2-x}Se$ solutions of chloroform, and is given per mole of 16 nm $Cu_{2-x}Se$ nanocrystals (see Supporting Information for calculations). The molar extinction coefficient reaches a maximum of 7.7×10^7 M^{-1} cm^{-1} at 970 nm.

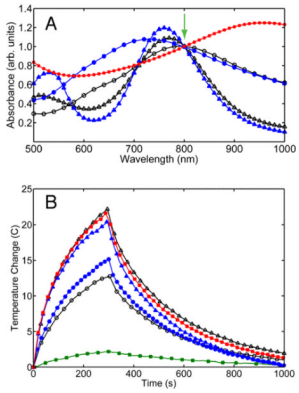

Figure 4.

(A) Absorbance spectra of polymer-coated $Cu_{2-x}Se$ nanocrystals (red solid square), commercial Au nanoshells (blue solid circle) and Au nanorods (blue solid triangle), and synthesized Au nanoshells (black hollow circle) and Au nanorods (black hollow triangle) dispersed in deionized water. All solutions were normalized to an optical density equal to 1.0 at 800 nm (green arrow). (B) The photothermal response of the dispersions in (A) obtained by irradiating 300 μL aliquots of each solution for 5 min with an 800 nm diode laser (6 mm spot size, fluence of 2 W/cm^2). The temperature was monitored with an infrared imaging camera. The laser heating of the water contributes approximately 2.5°C to the overall change in temperature in 5 min (green solid square).

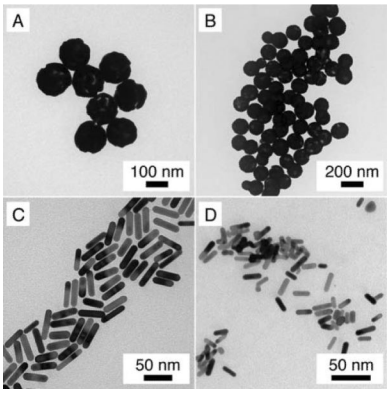

Figure 5.
TEM images of Au nanoshells and nanorods that were purchased from a commercial supplier and synthesized in-house. Synthesized Au nanoshells (A) are 135 nm in diameter, with an approximate shell thickness of 10 nm, while commercial Au nanoshells (B) are 145 nm in diameter, with a 7.5 nm thick Au shell. Synthesized nanorods (C) are 49 × 13 nm (aspect ratio: 3.8) and commercial nanorods (D) are 23 × 7 nm (aspect ratio: 3.3).

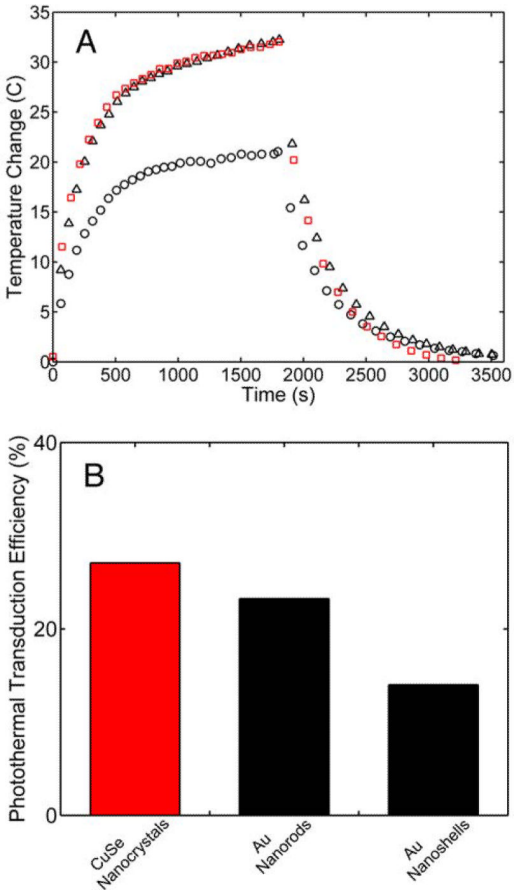

Figure 6.

Steady state heating data (A) for commercial Au nanoshells (black circles), commercial Au nanorods (black triangles) and $Cu_{2-x}Se$ nanocrystals (red squares). Dispersions of nanocrystals (300 μL) were irradiated with 800 nm light at low fluence (2 W/cm^2) using a 6 mm spot size. The thermal time constant τ_{out} was determined by fitting the temperature fall to Eqn (8). The photothermal transduction efficiency η, was then determined from the steady-state temperature rise using Eqn (9). (B) Plot of the photothermal transduction efficiencies for the $Cu_{2-x}Se$ nanocrystals, Au nanorods (commercial), and Au nanoshells (commercial).

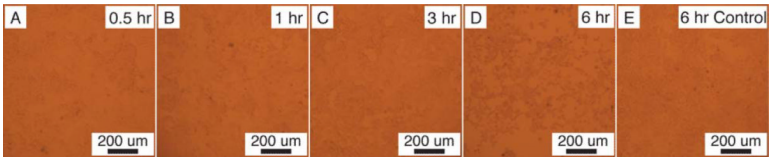

Figure 7.

Bright field optical microscopy images of human colorectal cancer cells (HCT-116) incubated with 39 mg/L polymer coated $Cu_{2-x}Se$ nanocrystals in PBS for 0.5 hr (A), 1 hr (B), 3 hr (C), and 6 hr (D). A control sample (E) was incubated for 6 hr and did not receive $Cu_{2-x}Se$ nanocrystals. Cells were incubated for the predetermined time and stained with Trypan blue to visualize cell death.

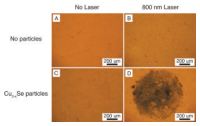

Figure 8.

Comparison of photothermal destruction of human colorectal cancer cells (HCT-116) without (top row – A and B) and with (bottom row – C and D) the addition of 2.8×10^{15} $Cu_{2-x}Se$ nanocrystals/L. Cells irradiated at 30 W/cm^2 with an 800 nm diode laser for 5 min (circular spot size of 1 mm) were stained with Trypan blue to visualize cell death and imaged with an inverted microscope in bright field mode. Significant cell death is observed with 30 W/cm^2 irradiation.

Table 1

Molar extinction coefficients (per mol of molecules or nanocrystals) of common photoabsorbers, including molecular dyes, direct bandgap semiconductors, and reported photothermal materials.

Photoabsorber	Dimension (nm)	Molar Extinction Coefficient (M^{-1} cm^{-1})	Wavelength (nm)
Rhodamine 6G[42]	Molecular	1.2×10^5	530
Malachite Green[42]	Molecular	1.5×10^5	617
CdX (X = S, Se, Te)[43]	r = 2	$\sim 2 - 5 \times 10^5$	At excitonic maximum
Carbon Nanotubes[4]	r = 0.6, L = 150	7.9×10^6	808
Copper Selenide	r = 8	7.7×10^7	970
Gold Nanospheres[44]	r = 20	$\sim 7.7 \times 10^9$	530
Gold Nanorods[45]	r = 5, L = 27	1.9×10^9	650
Gold Nanoshells[46]	$r_1 = 55$, $r_2 = 65$	$\sim 2 \times 10^{11}$	800